Comput Geosci (2007) 11:117–129
DOI 10.1007/s10596-006-9034-6

ORIGINAL PAPER

A distinct element simulation including surface tension – towards the modeling of gas hydrate behavior

S. Kreiter · V. Feeser · M. Kreiter · T. Mörz · B. Grupe

Received: 16 August 2006 / Accepted: 9 November 2006 / Published online: 16 December 2006

Abstract Gas hydrate bearing sediments are an integral part of the world's continental margins. Several tsunamigenetic continental slope failure events have been triggered by gas hydrates, but their mechanical behavior is poorly understood. In this work, we propose a method to simulate a surface tensed medium such as gas hydrate in soil, using distinct element method (DEM). For implementation in sediment pore size, we scaled up attractive particle interactions governing surface tension on molecular level. Several virtual experiments are used to benchmark the proposed method. A simulation of gas hydrate growth in sediment with differing grain sizes demonstrates the potential of the new approach.

Keywords distinct element method · gas hydrate growth · grain size effects · PFC · porous sediments · surface tension

S. Kreiter (✉) · T. Mörz
DFG – Research Center Ocean Margins, Bremen University, P.O. Box 330 440, 28334 Bremen, Germany
e-mail: skreiter@uni-bremen.de

V. Feeser
Institute of Geosciences, Christian-Albrechts-Universität zu Kiel, Hermann-Rodewald-Straße 9, 24118 Kiel, Germany

M. Kreiter
Max Planck Institute for Polymer Research, Ackermannweg 10, 55128 Mainz, Germany

S. Kreiter · B. Grupe
AG WUM, Technische Universität Berlin, Müller-Breslau-Strasse (Schleuseninsel), 10623 Berlin, Germany

1 Introduction

Gas hydrates are a solid high-pressure and low-temperature phase of water and small hydrophobic molecules, and the most common one in nature is methane hydrate ($8CH_4{\cdot}46H_2O$) [1]. Gas hydrates form in the pore space of the continental margin sediment. They frequently occur in all continental slopes in various textures, and there is evidence that they trigger huge continental slope failure events, some of which resulted in destructive tsunamis [2–4]. Gas hydrates are therefore a potential threat to the adjacent coastal regions and all human installations on the slope such as cables, pipelines, and oil platforms. The mechanical properties of such gas hydrate bearing sediments must be known to assess the natural hazards at the ocean margins. Moreover, this knowledge is invaluable in the specific permit procedures and planning of new off shore installations in gas hydrate areas.

The influence of gas hydrate growth and decay in the upper part of the continental slopes sediment on its mechanical behavior was fist discussed by McIver [5] and is the topic of recent research programs such as the construction of GHASTLI and HYDRATECH [6, 7]. A review of gas hydrate related actual research topics was recently given by Beauchamp [8]. Gas hydrate triggered slope failures are also a topic in the climate research community summarized in the "clathrate gun" hypothesis [9], clathrate being a synonym for gas hydrate.

Several mechanical concepts are proposed for gas hydrate growth and decay [5, 10–13]. Most of these concepts are only qualitative and until now there is no unifying model that describes the mechanical properties of gas hydrate bearing sediments. It is generally accepted that gas hydrates do have a substantial influence on the mechanical properties of the sediment; however, the character and extent of this influence is unclear. Some authors highlight a strengthening of the sediment during gas hydrate growth, due to the consolidation caused by volume reduction and cementation. Other authors emphasize the weakening and disintegration of the sediment during the gas hydrate decay, by water and gas release, volume increase, and reduction of the solid phase.

The textures of the natural gas hydrate observed in sediments testify that their growth in the sediment is a complex mechanical phenomenon. In fine-grained sediment, nodules and layers of different sizes have been found. Since they had been formed after the sedimentation, neighboring sediment was displaced during their growth [14]. In coarse-grained sediments, gas hydrates build a 3D framework cementing them together [15]. However, some fine-grained sediment that formerly contained minor amounts of gas hydrate, as proven by salinity measurements, showed no evidence of relic lenses or nodules [16]. Visual observation and electrical resistivity measurements of model sediment in a high-pressure container show that gas hydrate growth starts in the center of the interstitial sites between sediment grains [17–19]. This implies that gas hydrate is a nonwetting phase relative to sediment grains. The surface energy of nonwetting phases always results in forces in outward direction on the indenting phase. The high curvature in fine-grained sediment may lead to sufficiently high surface forces to push the neighboring grains away, building lenses and layers, whereas in coarse-grained sediments the curvature is low resulting in low surface forces and may allow the gas hydrate to grow around the grains building a rigid 3D network. Thus surface energies may explain the observed textures, and therefore surface tension of the gas hydrate crystal is accepted as a key factor for gas hydrate growth and resulting sediment textures [11, 13]. A quantitative description of this process is still lacking.

Nowadays, computer simulations are an established approach to complement or even partly replace experiments; thus, a reliable simulation of gas hydrate bearing and other sediments behavior would allow funded stability predictions for the continental slope, with only few sediment samples. In this report, we are presenting the first steps towards computer simulation of gas hydrate growth and decay in an arbitrary environment. Our aim is to contribute to the understanding of gas hydrate bearing sediments' mechanical properties and texture.

Although simulation of gas hydrate behavior was the motivation for this study, surface forces are acting at all phase boundaries and are therefore important for many geoscientific questions. Surface forces act on small scales and govern many processes such as crystal nucleation and growth, as investigated in petrology or the microbiological processes covered by biogeochemistry and biogeology. From the geotechnical standpoint, surface tension is known to lead to apparent cohesion of sand in partly saturated soils; furthermore, it affects the permeability for water and the bulk strength [20, 21]. Surface tension in fully saturated soils is, in general, of minor importance because the sand grains do not deform, but if additional phases such as oil or biopolymers are in the system, surface forces on these phase boundaries come into play. Ice and gas hydrate are special cases, because they are solid, but are susceptible to deformations during their growth and during long-term processes. As an introductory conclusion, surface tension in soils is an important issue responsible for many phenomena and applications including the growth and decay of gas hydrate. A new method for the simulation of surface forces may be useful in many geoscientific fields.

2 Concept of the simulation

In the following, the concept of the simulation is developed. It starts with an introduction of the simulation method, followed by the concept used to implement surface tension. We show how the used pair potential is chosen for optimum computational performance. Then, the connection between pair potentials and the surface tension of a two-dimensional discrete material is derived. Finally, some implementation-specific solutions regarding the repulsive part of the potential and variable disk size and cluster growth are explained, before moving on to the benchmark experiments.

2.1 Simulation framework: The distinct element method

The distinct element method (DEM) was chosen as the framework for the simulation, because it focuses on the grain and pore-scale – the scale on which the gas hydrate growth, decay, and interaction with the sediment takes place. DEM models can simulate large displacements and free shear failure planes; in this respect, they exceed the capabilities of classic finite element models. Using DEM, it is not possible to simulate a continental slope in true scale, but enough material can be simulated to measure changes in the bulk properties of the material in virtual experiments. These results can be directly compared to laboratory experiments or used as input for large-scale stability predictions.

DEMs are based on free-moving particles or elements that mutually interact [22]. The movement is governed by Newton's laws of motion. Since the particle interaction is modeled by a continuous potential, they can slightly overlap. Gravity, rigid walls, and other boundary conditions are used to implement a specific model setup. The simulation is fully dynamic in not only leading to a stable final state, but also in giving the whole development of the simulated process. The problem is solved in discrete time steps, and the minimum length of the time steps in the simulation is determined by the size of the smallest particle and the highest stiffness of the elastic particle interaction. Energy dissipation is provided by a "local" damping where the acceleration arising from collisions is reduced.

DEM is often used together with straightforward physical laws; for instance, magnetic forces were added to the method to simulate an ore separation process [23]. An electrostatic interaction has been implemented in a DEM simulation to optimize the toner transfer in laser printers [24]. Other interactions added were the interparticle forces of clays [25] and apparent cohesion from water menisci between sand grains [26]. The aim of this study was to extend possible interactions in DEM simulations by adding surface tension, a key factor of gas hydrate growth in sediments.

We used the software Particle Flow Code in two dimensions (PFC^{2D}) [27]. PFC is a commercial successor of "Ball" [22]; a description of software-specific implementation issues is given by Kreiter et al. [28]. This study uses a two-dimensional approach, since – for the development of a new method – calculation speed as well as implementation speed are critical.

2.2 Physics of surface tension and the implementation concept

Surface energy is defined as the energy needed to create a new surface (expressed in J/m^2). Surface tension is defined as the force perpendicular to a line on a surface (N/m). N/m can be expanded with m to J/m^2. In the Du Noüy ring experiment [29] described below, this tension force is measured. Although the term tension is mostly used to describe a force caused by the deformation of an elastic medium, thermodynamic surface effects also lead to a tension, referred to as surface tension. Thus, surface tension and surface energy have equivalent dimensions and values, and only semantic differences exist in placing more emphasis on the cause or on the effect of the same processes.

Analysis of surface energy reveals that the attractive interaction between molecules is the cause for surface energy and the related phenomena [30]. Molecules can be treated as particles, and the attraction underlying the surface energy can be directly implemented in DEM simulation. Individual modeling of real-scale molecules leads to very small particles, resulting in very small time steps and far too high computing times. Because of this performance issue, it is not possible to include molecules on their true scale ($\sim 10^{-10}$ m) in a simulation that also contains sand-sized particles ($\sim 10^{-3}$ m) of the sediment. Using up-scaled particles representing hydrate, the attractive interactions have to be scaled to fit the true surface tension. Although much larger than molecules, the hydrate representing particles have to be small compared to the smallest sediment grain.

Cluster size has to be variable to simulate the growth or decay of gas hydrate crystals in an arbitrary environment, and more specific in the pore space of marine sediment. The interaction between this cluster and the environment has to be only dependent on the known surface tension of gas hydrate. The purpose of ensuring this condition is to enable the simulation of virtual gas hydrate bearing sediments, in which texture and stress field development can be analyzed in virtual geotechnical experiments as preliminary shown in [28, 31].

The concept used includes the use of different disk sizes within the gas hydrate representing particle clusters for theoretical and practical reasons. A material composed of disks of the same radius exhibits unwanted pseudo-crystalline properties, resulting in preferential cleavage directions, anisotropic elasticity, and shear strength. In effect, the growing procedure for gas hydrates, which is described below, was designed with the possibility of creating new disks with minimal disturbance while retaining a decent performance. This mechanism involves the use of small and big disks.

2.3 Selection of the used pair potential

The interaction between the particles is given by a pair potential and this potential has to be governed by surface energy. This pair potential has to meet several conditions, such as being zero at infinity and having a minimum value at the particle diameter; however, there are numerous potentials that match those conditions. The length of time steps in the simulation is determined by the size of the smallest particle and the highest stiffness of the elastic particle interaction. Small particles and high stiffness result in small time steps and prohibitively high computing times. The pair potential determines the "stiffness" of the interaction between the gas hydrate representing particles. Another important condition for the physics of surface tension and computational performance is the range of the potential: it should be short [30]. Low stiffness and short range are somewhat contradictory demands for the potential. The last consideration is that the potential should be as simple as possible. The used potential is chosen to match the conditions as best as possible.

In our study, we chose the Mie potential [30] as simple pair potential with one attractive and one repulsive term. It has the form:

$$w(r_{\mathrm{d}}) = -Ar_{\mathrm{d}}^{-n} + Br_{\mathrm{d}}^{-m}. \tag{1}$$

where w is the potential, r_{d} is the distance between two particle midpoints, and A, B, m, and n are constants with the condition $n>m$ and $m>3$. In molecular dynamic simulation, a Mie potential with $n=12$ and $m=6$, the Lennard–Jones potential is often used. We examined the key properties of the Mie potential family to choose the best potential for our simulation.

The potential has four independent variables and can be written in the form:

$$w(r_d) = -Ar_d^{-n} + Br_d^{-m} \Leftrightarrow w(r_d) = A\left(-r_d^{-n} + \frac{B}{A}r_d^{-m}\right) \tag{2}$$

The right side of equation (2) shows that parameter A can be regarded as a scaling factor, which is necessary to adjust the strength of the interaction, and parameter B/A is then fixed if a potential minimum is dictated by the particle size, as explained below. That leaves m and n for optimization for low stiffness and short range.

From the potential, a stiffness D_r can be derived in analogy to the spring stiffness D in Hook's law (3) and its underlying potential (4).

$$F = -Dr_d \tag{3}$$

$$w_{Hook}(r_d) = \frac{1}{2}D(r_d - \sigma)^2 + w_0, \tag{4}$$

F is the repulsion force, r_d is the displacement, w_{Hook} is the underlying potential, and σ is the distance (where w_{Hook} has a minimum value). For a spring, the stiffness is a constant and therefore independent from r_d. For an arbitrary potential w, stiffness $D_r(r_d)$ is more generally defined as the derivative of the force with respect to the displacement r_d.

$$D_r(r_d) = \frac{dF(r_d)}{dr_d} = \frac{dw(r_d)}{dr_d^2} \tag{5}$$

The Mie potential's stiffness increases with decreasing distance. As a typical stiffness value for the comparison of Mie potentials, the equilibrium situation, i.e., the stiffness at the potential minimum, is considered.

The range of the potential is infinite, but the interaction energy decreases rapidly with distance. An effective potential range $r_{d1/2}$ is defined, where the absolute value of the interaction energy E of one particle with a homogeneous and infinite approximated medium of other particles has decreased to half of its value at the minimum E_{min}.

$$E(r_{d1/2}) = E_{min}\frac{1}{2} \tag{6}$$

with

$$E(r_d) = \int_\sigma^\infty w(r_d) 2\pi r_d \rho d(r_d) \tag{7}$$

where ρ is the particle density of this medium and σ is the distance of the energy that reaches its minimum. The integration sums up the interactions for the whole area outside the distance σ to infinity.

As a note to readers who are used to geotechnical notations, we want to stress that the used σ has no connection to the stress notation in geotechnics. The notation σ for the pair potentials minimum distance is adopted from Israelachvili [30], and a very common notation in molecular and surface science was also used by Allen and Tildesley [32].

An analysis of all possible exponent combinations of m and n from 3 up to 12 was performed with A and B adjusted to constant particle size and a constant surface tension, as derived below. The resulting effective distance is plotted versus stiffness at contact in figure 1, with one data point for each Mie potential with exponents n and m. In general, a high exponent m leads to a short range and a high exponent n to an increase in stiffness. As a compromise between low stiffness and short range, the potential has to be as low and left in the diagram as possible. Finally, the potential with $n=6$ and $m=7$ was chosen (figure 1). Another possibility would have been $n=7$ and $m=8$.

2.4 Linking the pair potential to surface tension

Now, the chosen pair potential is linked to the surface energy for the two-dimensional simulation. In two dimensions, surfaces are reduced to contour lines, but in analogy to the physical 3D problem, "surface" is used in this paper for the length of the phase boundary in 2D. Treatment of the potential in three dimensions involves only minor changes.

Although gas hydrate in the simulation consists of arbitrarily placed particles of different sizes, for the derivation of the pair potential the geometry was approximated by a close packing of equally sized disks. The surface energy γ of a material can be calculated as energy E_{sep} needed to separate two surfaces of the material, normalized by the new created surface area [30]. The interaction potential on the molecular level as well as the upscaled model potential are of very short range; therefore, as a first approximation only the nearest neighbors are considered. Surface energy is deter-

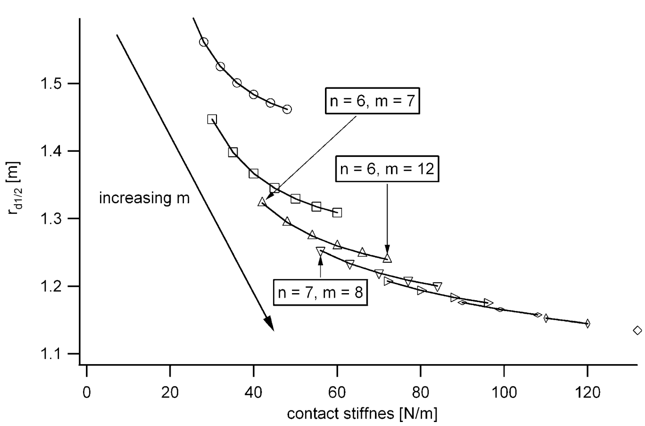

Figure 1 Effective potential range $r_{1/2}$ versus the stiffness at contact for Mie potentials with exponents n and $m<12$. The exponents are indicated for the Lennard–Jones potential and the chosen potential.

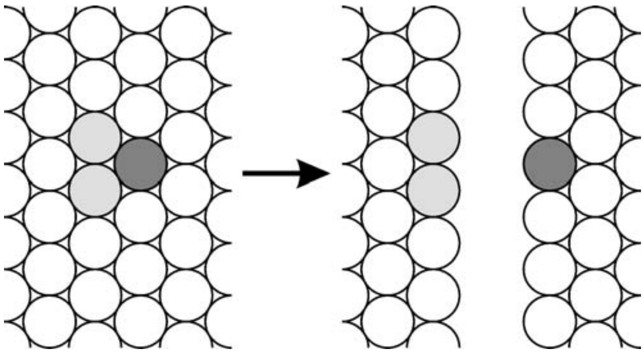

Figure 2 Creating a new surface in a close packed assembly: The dark gray disk and every other disk loses two neighbors, marked in light gray for the case of the dark gray disk.

mined by considering the process sketched in figure 2. A close packed array of disks is separated. During the separation process, each disk loses two of its six nearest neighbors, and two times the disk diameter new surface is created, one on each side of the gap (figure 2).

We define here the disk diameter of two equally sized disks to be the pair potential minimum distance σ. This is just a definition, because particles with an infinite interaction range have no clearly defined size (the average midpoint distance between two neighboring particles in an ensemble is dependent on many factors). The actual movements of the particles modify the midpoint distance over time and space. Although the movements are mainly determined by the pair potential between the nearest neighbors, they are also influenced by interaction with farther neighbors – in terms of overall pressure and excitation from the surrounding material. For short-ranged potentials, not too vigorous excitation and low external pressure the average disk diameter does not differ much from the distance of the minimum of the pair potential, therefore the definition is reasonable. Accepting this allows us to calculate the separation energy E_{sep}:

$$E_{\mathrm{sep}} = 2w(\sigma), \tag{8}$$

where w is the Mie potential (1); the surface energy γ therefore amounts to

$$\gamma = \frac{E_{\mathrm{sep}}}{2\sigma} \tag{9}$$

The potential minimum σ for two particles, with different radii (r_1 and r_2), is defined as

$$\sigma = r_1 + r_2 \tag{10}$$

The potential minimum is where the derivative is zero, and Mie potentials have only one extreme value which is a minimum.

$$\frac{-\mathrm{d}w(\sigma)}{\mathrm{d}\sigma} = 0 \tag{11}$$

The insertion of (8) in (9) leads to the combination in (11), and the exponents n=6 and m=7 in (1) and rearranging yields the following equations for A and B.

$$A = 7\gamma\sigma^7 \tag{12}$$

$$B = \frac{6A\sigma}{7} \tag{13}$$

The attractive force is calculated by:

$$F(r_{\mathrm{d}}) = \frac{\mathrm{d}w(r_{\mathrm{d}})}{\mathrm{d}r_{\mathrm{d}}} = -\frac{6A}{r_{\mathrm{d}}^7} + \frac{7B}{r_{\mathrm{d}}^8} \tag{14}$$

where r_{d} is the distance between the centers of the disks and F is the force between the disks.

2.5 Implementation-specific issues

The simulation is designed for differing and dynamically changing disk sizes (10), so A and B are calculated at each time step for every pair. The potential is only applied for separated disks (i.e., $r_{\mathrm{d}}>\sigma$). For interpenetrating disks the repulsive force is derived from a standard spring type potential (4) provided by the software package. The use of spring type potential allows users to define a maximum stiffness and so the simulation can benefit from the automatic time step detection of the software package, which is based on the theory of multiple mass spring systems [27]. A simulation with a theoretically infinite stiffness would necessitate the implementation of another time step detection scheme, with the risk of adding overhead and producing erroneous or unstable results. The interpenetrating stiffness was first set to the stiffness at contact, but that produced large interpenetration of the disks. Several simulation runs revealed that a stiffness of four times the Mie stiffness at contact results in satisfactorily low interpenetration and reasonably long time steps. The resulting force and potential are shown in figure 3, and the stiffness in figure 4.

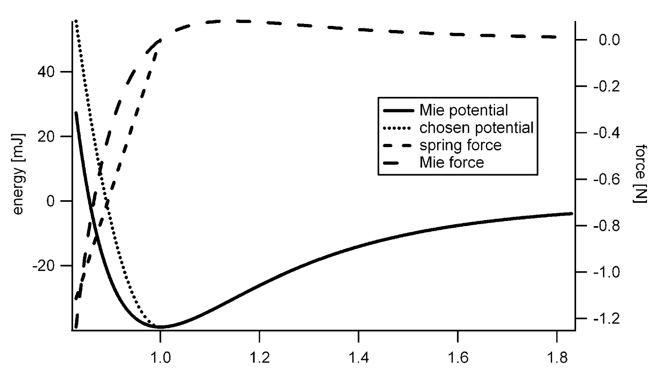

Figure 3 Distance dependence of the Mie potential with the exponents n=7 and m=6, and the resulting forces for two disks with a diameter of 1 m and the surface tension of 0.039 J/m^2.

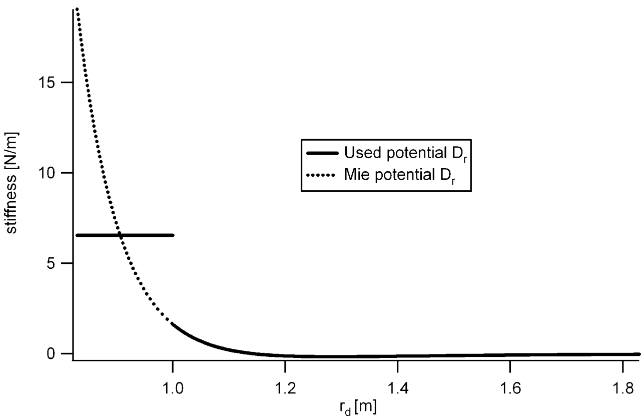

Figure 4 Distance dependence of the stiffness of the chosen and the Mie potential of figure 3.

The chosen potential has a discontinuity in the stiffness, but that causes no problem during the simulation because the underlying force is continuous, and this is the term (value) used in the simulation. The underlying potential is actually differentiable.

For large particle ensembles, calculation of the interaction between every pair intolerably degrades the performance of the calculation; therefore, the possibility to cut off the potential at a certain distance was included in the code and the cutoff distance is chosen after the experiments described below.

Growth of the gas hydrate is simulated by two mechanisms: (1) the gas hydrate representing disks expand; (2) disks exceeding a maximum radius are substituted by three small disks (figure 5a). The large and small disks are termed child and parent, respectively. This maximum radius is defined as a fraction of the minimum radius of the surrounding nonhydrate disks; in this work, this fraction was set to 1/30th. The new "child" disks fall completely inside the circle defining the parent disk to avoid the forces that would result from overlap with their neighbors. This procedure reduces the overall area of the disks; this reduction is compensated by the fast growth of child disks during the following calculation steps.

The decay in three disks is a compromise between minimum area loss and maximum resulting child radius (figure 5b). The main breaks in the area fill ratio curve is from two to three and from six to seven children, whereas the child radius shrinks nearly linearly form two to six children. Therefore, three child disks were taken as a best option.

To avoid shock wave formation resulting form fast particle growth, the radius expansion in one time step, Δr, has to meet two conditions: First, the energy introduced by the possible overlap generated by the expansion of the radius is set to a fractional amount *fract* of the separation energy. The overlap energy is calculated after (4), whereas r_d–σ is replaced by Δr_E. A factor of 2 is introduced to account for the possibility of two expanding disks in contact. Separation energy E_{sep} is obtained by inserting (1) in (8).

$$\left(-A\sigma^{-6} + B\sigma^{-7}\right)\mathrm{fract} = \frac{1}{2}D(2\Delta r_E)^2 \qquad (15)$$

yielding

$$\Delta r_E = \frac{\sqrt{\mathrm{fract}\left(-A + \frac{B}{\sigma}\right)}}{\sqrt{2D\sigma^3}}. \qquad (16)$$

Note that the disks expand; therefore, Δr is positive. Second, the radius expansion must be smaller than the distance that this particle moves in one time step Δt. This distance, Δr_t, is approximated by using (3), Δr_E from (16), and the force–acceleration law by

$$\Delta r_t = \frac{D\Delta r_E \Delta t^2}{2\pi\left(\frac{\sigma}{2}\right)^2\rho}. \qquad (17)$$

When performing the disk's radius expansion, we use either Δr_E and Δr_t for whichever is the lower value in each case. A fractional amount of 0.2 was used for the calculations of (16) in this paper.

The growth mechanism was only used for the simulation of gas hydrate growth in the sediment. Gas hydrate decay can be simulated by shrinking and deleting of single gas hydrate disks.

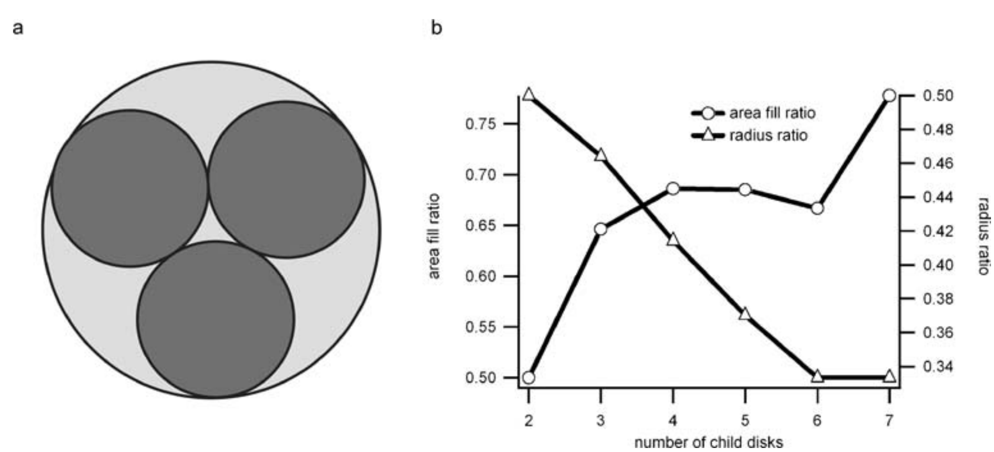

Figure 5 (a) Geometry of the disk splitting process. Parent disk and child are shaded in light and dark gray, respectively. (b) Key parameters that guided the choice of child to parent geometry during the splitting and replacement process. Area fill ratio: area of parent disk minus sum child disks area normalized by the parent disk area. Radius ratio: child disk radius divided by parent disk radius.

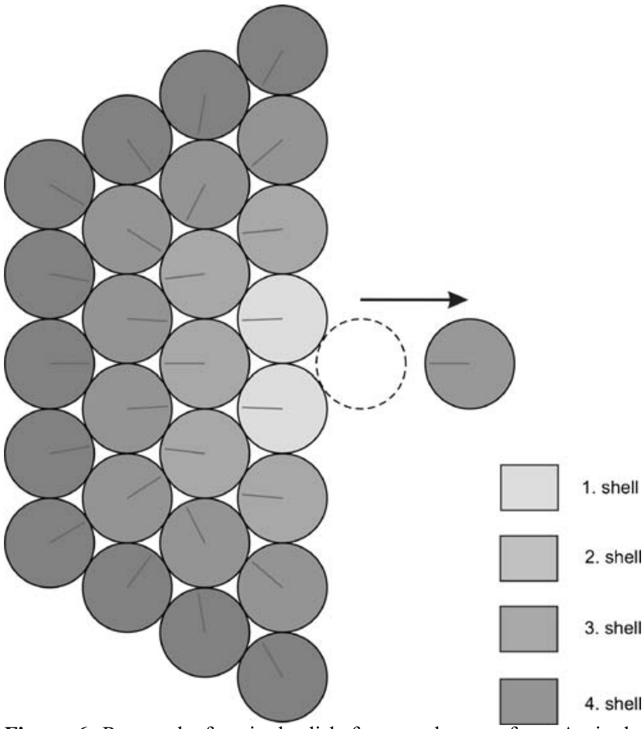

Figure 6 Removal of a single disk from a plane surface. A single probe disk moves to the right, the initial position is shown in dashed lines, the different shells of the close packed disk ensemble are indicated by gray shades. The direction of forces acting on the disks is indicated by dark lines starting in the center of disks.

3 Experiments

The theoretically derived potential was benchmarked by simulations described in the following section. The experiments start with close packed ensembles, proceed to random ensembles, incorporate free movement, and finally simulate the growth of gas hydrate in a sediment pore.

3.1 Close packed ensembles

The first experiment was designed for two purposes: (1) to test the general usability of the simulation code and (2) to investigate the influence of disks more than a diameter away in a regular, but reasonable geometry scenario. For this purpose, the energy needed to detach one disk from a close packed ensemble of equally sized disks was analytically calculated and simulated. One probe disk is placed in contact to an ensemble of close packed disks. An experiment with four "shells" is shown in figure 5. Simulations were performed for analogous geometries with 1, 2 to 10 shells. The pairwise attractive interaction derived above (14) is applied to all disks. No free movement is permitted, the position of the close packed disks is fixed, and the probe disk is moved apart in a predefined number of time steps to a distance of 10 times the diameter of one disk. The energy E required to overcome the attractive force is recorded during the experiment by reading out the force and the displacement r_{d} for each calculation step:

$$E\sum_{\text{steps}}\vec{F}\vec{r_{\mathrm{d}}} \tag{18}$$

To illustrate the internal interactions, the direction of the resulting attraction is shown for each disk.

Figure 7 shows the resulting energies of the virtual experiments and the analytical solution of the equivalent problems using equation (1) and the known geometry relations of the close packing. In contrast to the simulation, where the separation stops at a distance r_{d} of 10 times the disk diameter, the analytical calculation is solved for infinite separation.

Constants A and B are calculated after (12) and (13) to match a surface energy of 1 J/m. The diameter of the disks is 0.5 m, thus the separation energy of the two nearest-neighbor disks is expected to be 1 J (8). The simulation with one shell is equivalent to the geometry used for the derivation (compare figures 2 and 6). In this case, the simulation with 2000 steps yields 1 J and therefore correctly reproduces the derivation geometry.

Calculations with more layers show that the outer shells increase the separation energy to 132.9% of the value obtained when considering next-neighbor interactions only. The difference corresponds to approximations used during the derivation. It confirms that most of the energy arises from the interaction with the nearest neighbors, but also that a minor and nonnegligible amount of energy is contributed by the farther surrounding. However, the contribution of layers beyond layer 4 is negligible, reflected in constant values of the separation energy of layer 4 or greater (figure 7).

Since naturalistic models always include numerous particles, resulting in large number of layers, a correction is needed. For the case of multiple close packed disks, the multiplication of the input surface tension with 1/1.329 gives

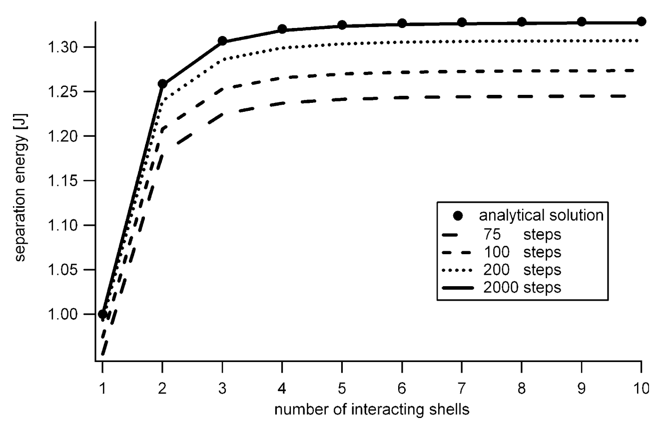

Figure 7 Diagram of the separation energy plotted versus the number of shells of a close disk packing interacting with the probe disk (q.v. figure 6). Filled circles show the energy derived from the analytical solution; lines show the results of DEM simulation using different numbers of steps.

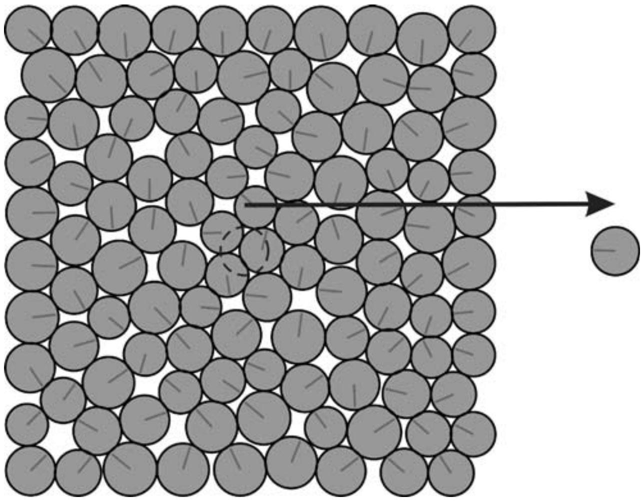

Figure 8 Snapshot of a virtual experiment involving 110 randomly assembled disks with a ratio of 1.3 between the largest and the smallest disk. The probe disk is moved out of the square disk ensemble, and its starting location is indicated by the dashed contour; the arrow shows the movement of the disk. The direction of attractive forces acting on disks are indicated by the dark lines starting in the center of the disks.

the desired result. Particle arrangements that differ from close packing (e.g., as in figure 8) require other correction factors.

Furthermore, it can be noted that the simulation reproduces the analytically calculated energies as perfect as desired if enough time steps are run. The error introduced by coarse time step resolution adds in this case up to a maximum of about 10%.

3.2 Random ensembles

The next experiment was carried out to evaluate the influence of complex disk arrangements, which cannot be treated with simple analytical calculations. It was designed to check how a randomly assembled disk packing and different disk sizes influence separation energy. Another question was, how many disks are required in an ensemble of disks to obtain constant separation energy? The fixed, artificial boundary conditions, where only one disk is allowed to move in a given mode, were retained for reasons of simulation efficiency and to exclude the influence of particle movements.

A disk is moved out of a square of randomly assembled disks with varying particle diameters (figure 7). A block of disks with a random radius distribution was generated via the standard radius multiplication procedure of PFC^{2D} [27]; subsequently, the positions of the disks are fixed. A probe disk is generated in the center of the block, and moved outward, while recording the energy of the attractive forces. Repulsion forces due to overlaps are not recorded.

The energy required to move the probe disk against the attractive forces is calculated using equation (18) (figure 9). The resulting energy is given as a function of the probe position in figure 8. Inside the particle ensemble, the energy oscillates around zero, and after the probe reaches the edge of the ensemble the potential rises rapidly to a constant level. Fluctuations inside the block depend on the geometry; therefore, different starting geometries have slightly varying energy levels. This potential of several disks with random relative positions can be compared to the smooth potential of two disks in figure 3.

The extraction energy of the disk was then normalized to the equivalent new surface produced to obtain a value that can be compared with the surface energy. The surface was calculated according to equations (8) and (9) by assuming that an average of six neighbors has been lost (see figure 2). Looking at the derivation, where two close packed materials are separated, this is equivalent to a surface of six times the diameter of the disk (figure 2). The result of a series with different numbers of disks is shown in figure 10.

It can be seen that ensembles of 10–20 disks and more exhibit constant normalized extraction energy, so an ensemble should at least contain 10 disks. The observed maximum extraction energy is higher than the energy derived from a nearest-neighbor interaction because of the

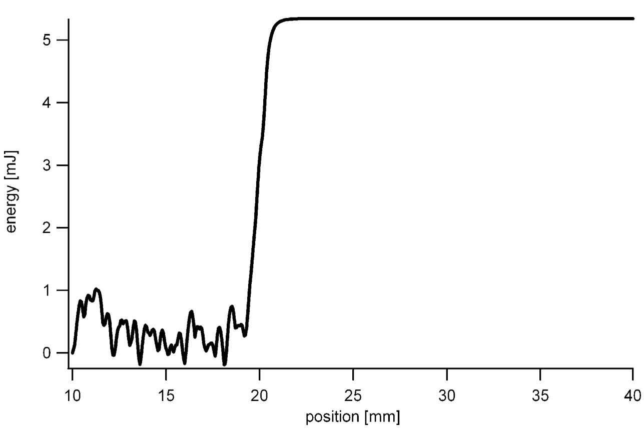

Figure 9 Energy needed to move the probe disk against the attractive potential. Box size 20 mm, middle of the box is at 10 mm.

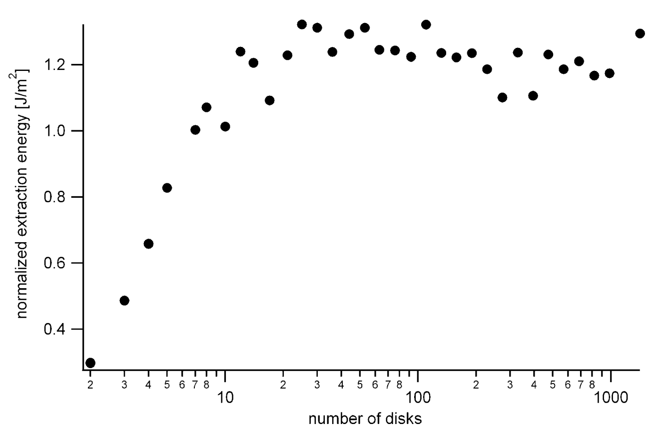

Figure 10 Normalized extraction energy vs. number of disks in the square disk ensemble. Note the log scale on *x*-axis.

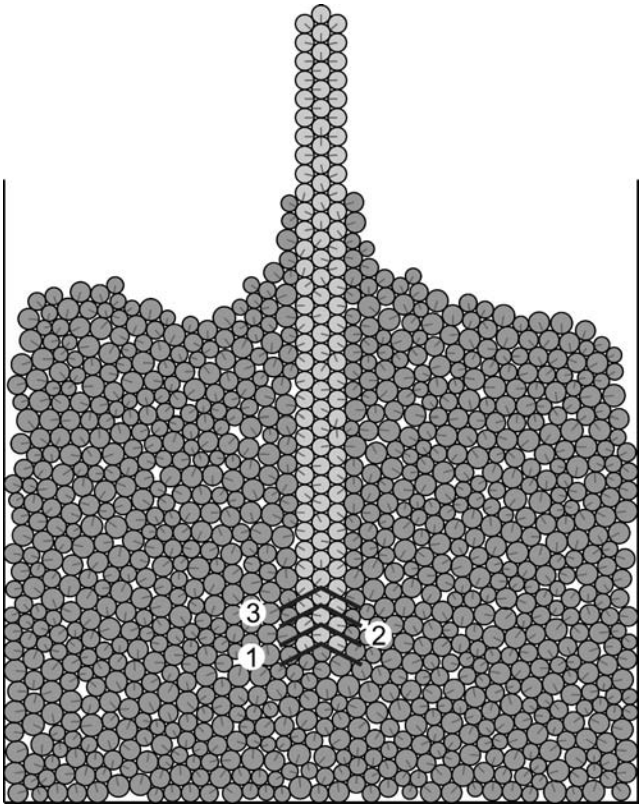

Figure 11 Setup of the virtual Du Noüy ring experiment with 1000 disks. The fluid film is represented by the block of light gray dense packed disk in the middle of the experiment. Dark gray lines starting in the center of the disks indicate the direction of forces acting on the disks. Note the climbed meniscus around the "fluid film" and the convex shape near the noninteracting walls. The average kinetic energy was lowered in order to obtain a well-defined free minimum energy surface. In the lower part of the rigid probe, the distribution of disks in horizontal layers is illustrated.

long-range influence of the potential, as already observed in the previous section, although lower than that in the close packed case (figure 7). The packing appears looser because the lacking particle movement results in large overlaps,

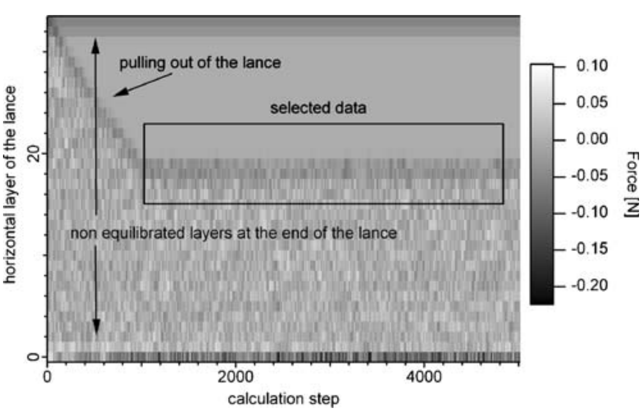

Figure 12 Plot of attractive forces on each horizontal layer of the probe as gray shades – the darker the color, the higher the force in downward direction. The framed area corresponds to layers and time steps taken for further evaluation. In the first 1000 steps, the probe is moved upward, out of the particle ensemble.

which are equivalent to void space for this special setup. The long-range interaction and packing correction factor is, in this case, approximately 1/1.2.

The cutoff distance of the potential was examined via a similar series of experiments leading to a distance at least 3 times the particle diameter for acceptable results and 6 times for quasi-perfect matching with a non-cutoff potential; the latter was chosen for the following simulations.

The influence of the size of the probe was explored during another experimental series. A smaller-than-average probing disk results in larger observed extraction energy, and a larger-than-average probe disk diameter results in smaller observed extraction energies. Further experiments were carried out to test the influence of the ratio of the largest to smallest disk radius while using the average radius for the probe. These experiments show that only the scatter of the measurement changes. To summarize, we state that the use of different disk sizes introduces artifacts if we focus only on single disks, and that these artifacts average out when the whole ensemble is considered.

3.3 Du Noüy ring experiment – free moving ensemble

Bearing in mind that the simulations should reproduce realistic experimental conditions, a virtual equivalent of the du Noüy ring experiment [29] was developed. In this experiment, the surface energy is determined by measuring the maximum force the fluid exerts on a film that is held by a ring until the fluid film ruptures. The fluid is simulated by a box full of freely moving disks (figure 11). As equivalent of the fluid film, a rigid probe of close packed disks is used, and medium-size disks of the probe were used to avoid sampling bias that arises from using varying disk sizes. The attractive interaction is applied between all disks and the correction factor of 1/1.25 was used.

Several failed experiments have shown that an adjusted attractive potential alone does not suffice to simulate a surface tensed fluid with a particle method. The inter-

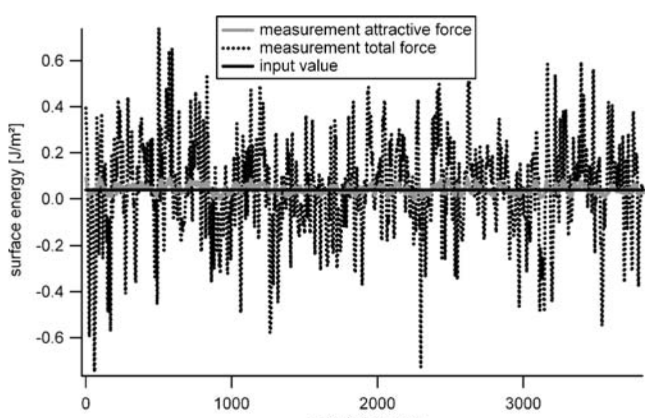

Figure 13 Surface energy calculated from the attractive force and total force measurements.

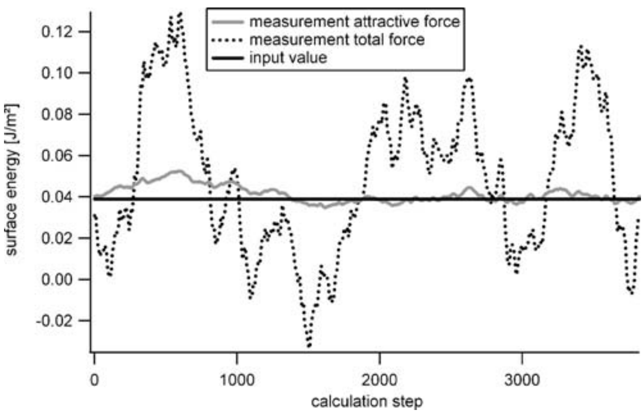

Figure 14 Moving average of 500 values of the surface energy calculated from the attractive force and total force measurements.

locking of particles inhibits the formation of minimum energy surfaces, and the material exhibits a brittle type of failure and is in a sort of solid state. Neither the resulting geometries nor the surface energy measured by the du Noüy method is realistic. Our solution was to "melt" the material to the fluid state. As the underlying principle of temperature is the average kinetic energy of molecules, we added random particle movements to the disk ensembles. A random number generator is used to create velocity vectors with random directions that are, in turn, assigned to the disks until the desired average kinetic energy level is reached. Slight damping is applied to dissipate the energy added by other means to the system. The slight energy dissipation is balanced by adding a few new random movements and the average kinetic energy is held constant. As a result, the material deforms in a nonbrittle way and forms minimum energy surfaces.

The average kinetic energy can not be related to meaningful Kelvin temperature, because the simulation is scaled up and the moving particles have differing masses. The average kinetic energy needed to attain a fluid state is expected to vary with the disk size.

Simulation of the fluid film by close packed disks is a simplification, which has to be kept in mind for the analysis of experimental results, and implies several consequences.

First, the ends of a probe built by a close packed ensemble are not in equilibrium, because of the long-range interaction of the disks. Although the nearest neighbors to the disk at the end of the probe are in contact and therefore exert no forces, the farther neighbors attract the probe in an inward direction and cause nonequilibrium forces. These nonequilibrium forces have shown to be in the range of forces to be measured and can not be neglected. They can be seen from the directions of the forces of the top of the probe in figure 11, and from the upper and lower margins of the gray shade plot in figure 12. In the middle part of the probe, the disks are free from this artifact and therefore this part is used for further analysis.

Second, the density of the close packed ensemble is in general not the same as the density of the surrounding bulk material particle ensemble, and the disks forming the probe are not in random movement. This leads to vertical buoyancy forces originating from the sum of the collisions, which have been found to sum up to a significant artifact for long probes.

To reduce this artifact, the part of the probe used for the measurement has to be as short as possible, but has (nevertheless) to include all surface effects. Therefore, a gray shade plot is generated to visualize the force development of the probe in space and time (figure 12). The probe is divided into layers as drafted in figure 11, where every area in the plot corresponds to a defined time step and a defined layer of the probe. The plot is divided in two areas: one showing the same shade and another with fast-changing gray shades. The first area corresponds to times and vertical sections of the probe where there is no interaction with the free-moving disks; the second corresponds to times and sections where the changing positions of the disks lead to quickly changing forces and shading. The top and the bottom borders of the figure correspond to the ends of the probe, and the differently shaded bands there are caused by the end artifacts described above. In the beginning of the experiment, the probe is fully immersed in the box containing the free-moving disks and is then pulled out, which can be observed by the triangular shape of the evenly shaded part from the left to the right. The zone

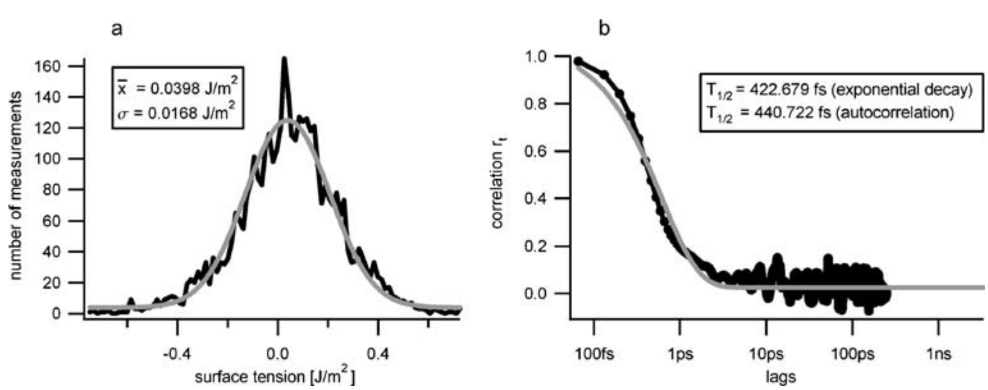

Figure 15 (a) Frequency distribution of data shown in figure 13. The gray line is a fit of the data to a normal distribution mean x value and standard derivation are shown in the inset. (b) Autocorrelation of the same data. An exponential decay (gray line) is fitted to the data. $T_{1/2}$ indicates the half-life of the correlation.

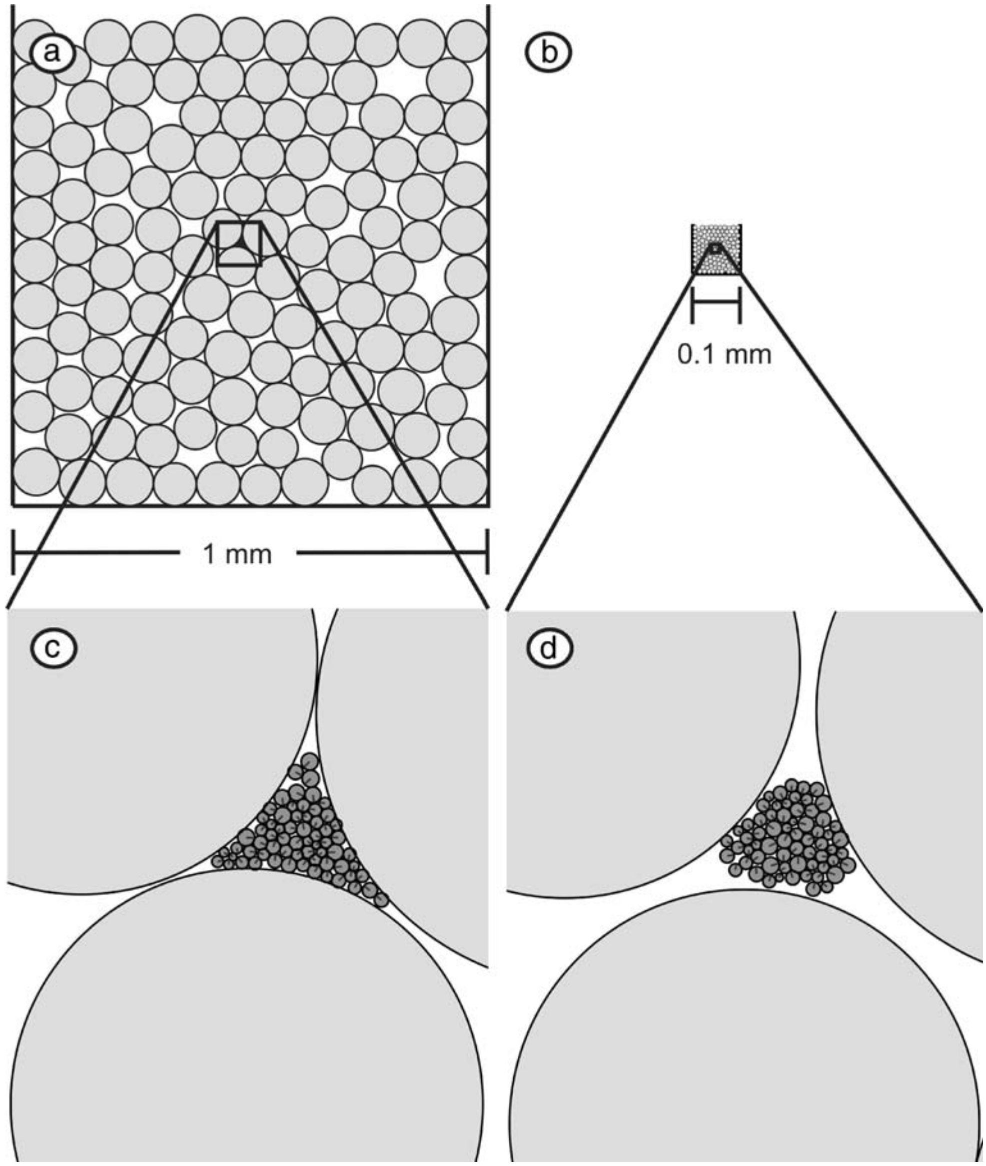

Figure 16 Geometry after gas hydrate growth in two virtual sediment samples with differing grain size. (a and b) Configuration of the sand (~0.091 mm diameter) and silt (~0.0091 mm diameter) grain size experiments, respectively. (a) and (b) are shown on the same scale, indicated by the scale bars. (c and d) Details of the gas hydrate in the sand and silt pore space.

influenced by the surface forces can be seen from darker shading near the interface of the two main areas. The vertical probe section and time period used for further analysis in the experiment is shown as a rectangle.

The measured surface energy of the experiment is shown in figure 13. The total force and attractive forces measured, and the surface energy is derived for each of them by

$$\gamma = \frac{F}{2} \tag{19}$$

In figure 14, the moving average of the same data is shown. The measurements oscillate around the value that was used as input value for the simulation to calculate the particle interaction. This proves the applicability of the method to free moving ensembles and especially for the simulation of gas hydrate growth in confined pore space.

The probability distribution of the extracted surface energies shows a normal distribution, and the mean value matches the simulated surface tension of 0.039 J/m^2 (figure 15a). The autocorrelation shows that the measurements have a red noise overprint. The correlation decay cannot be exactly fitted with an exponential decay law, but nevertheless shows a similar behavior. From the autocorrelation, a typical half-life period ($T_{1/2}$) of 440 fs is recorded, which corresponds to about seven calculation steps (figure 15b). This period must be simulated at least several times, until the systems' reaction to an applied disturbance can be expected or a statistically independent value can be obtained.

3.4 Gas hydrate growth in the pore space

The last virtual experiment simulates gas hydrate growth in the pores of sediments with different grain sizes. It is more a proof on concept that a thorough analysis of gas hydrate growth in the sediment is currently pursued and will be the subject of a further study. Simulation of the sediment grains is kept simple by using rigid round grains with a stiffness of 3.8×10^{10} Pa and a friction of 0.3, simulating quartz-dominated sediment with medium rounded grains. The gas hydrates surface tension is 0.039 J/m^2 [33]. We used 0.078 J/m^2 for our two-dimensional simulation, because the interface pressure for a given radius of a sphere is double the interface pressure of a cylinder. A tiny disk acting as seed for gas hydrate crystal growth was added in the pore space and additionally to the pair potential; the growth mechanism was used.

A sand- and a silt-sized specimen were prepared, both having the same relative initial geometry. The amount of gas hydrate that has grown was scaled with grain size, and the geometry after gas hydrate growth in the pore is shown in figure 16.

In fine-grained sediment (figure 16d), the gas hydrates surface force is pushing the neighboring grains away; in the coarse grained sediments (figure 16c), the pore space is completely filled. This is in good agreement with observations in nature, as discussed in the Section 1.

Although we think that our method is valid for simulation of gas hydrate texture, there are problems with the 2D approach that cannot be overcome. There is no way to transfer gas hydrate disks from one sediment pore in the neighboring pore without moving the sediment grains; in other words, the pore space in 2D is not connected. As a consequence, the simulation of a 3D sediment cementing network is impossible and the simulation of vast amounts of gas hydrate in coarse sediment in 2D should be regarded with caution.

4 Summary

Attractive forces for simulating surface tension using an ensemble of distinct elements are derived for arbitrary disk geometries and scales, and are tested in a series of experiments.

The experiment with hexagonal close packing revealed that (1) simulation reproduces the geometry used for the derivation perfectly, and (2) a slight long-range influence and packing correction is necessary to correct the surface energy. The need for a slight correction is consequently observed in all other experiments.

Simulation of random packing revealed four important results: (1) The method is applicable to random packing. (2) The minimum number of disks for a cluster with bulk properties is about 10. (3) Use of differently sized disks introduces artifacts when focusing on one disk, but these artifacts average out when regarding a whole cluster with a balanced disk size distribution. (4) No error is introduced by cutting off the interaction at six times the disk diameter and it is possible to cut off at half this value without significant loss of precision.

Simulation of the Du Noüy ring surface energy measurement revealed that correct surface energy alone does not lead to minimum energy surfaces and that random particle movements, emulating temperature, are necessary to achieve this goal. With the use of a correction factor and emulated temperature, a fluid with arbitrary surface energy can be simulated by the DEM method.

Simulation of gas hydrate growth in the sediment showed convincing gas hydrate behavior, but also illustrated artifacts that are introduced by representing a 3D world in 2D.

5 Conclusions

A method to simulate a surface tensed medium with DEM is developed and the applicability of this approach is shown with a series of benchmark experiments. Potentials derived from only the nearest neighbors have to be corrected for long-range effects and the application of random particle movement – an equivalent of temperature – was identified as a crucial point for realistic cluster behavior.

There are problems in the restriction to two dimensions that cannot be overcome. However, we think that the proposed method is applicable for moderate gas hydrate volumes and fine grain size.

For a simulation of cementation, it is necessary to move to a 3D simulation, which is perfectly possible with the same implementation strategy. However, a 3D simulation is expected to require more computational power than a 2D simulation for the same number of elements, and the element number will scale with the cube and not the square of the problem size.

We think that other problems in which surface tension is important may benefit from the described method, such as partly saturated soils, multiphase flow, and growth of other concretions in the sediment.

Acknowledgements The initiation and initial funding of DEM modeling of hydrate growth in porous sediments trace back to the work group Ingenieurgeologie at the Institute of Geosciences, Kiel University. Further model development at the Technische Universität Berlin was funded by the German Federal Ministry for Education and Research (BMBF) within the "Geotechnologien" research program "Gashydrate im Geosystem" grant no. 03G0560A. The benchmark experiments and fine-tuning was funded by the DFG – Research Center Ocean Margins (RCOM) of Bremen University (No. RCOM XXXX). We want to thank Lothar te Kamp from Itasca Consultants GmbH for helping with C++ problems during the implementation. The authors are solely responsible for the contents of this paper.

References

1. Sloan, E.D.: Clathrate Hydrates of Natural Gases. Marcel Dekker, Inc., New York, Basel (1998)
2. Mienert, J., Posewang, J., Baumann, M.: Gas hydrates along the northeastern Atlantic Margin; possible hydrate-bound margin instabilities and possible release of methane. In: Henriet, J.P., Mienert, J. (eds.) Gas Hydrates; Relevance to World Margin Stability and Climate Change, pp. 275–291. Geological Society of London, London, UK (1998)
3. Bondevik, S., Harbitz, C.B., Dawson, A., Dawson, S., Løvholt, F., Mangerud, J., Svendsen, J.I.: The Storegga Slide tsunami along the Norwegian coast – from the geological record to numerical simulations. http://www.ibg.uit.no/~stein/abstarct02fig_NPF2002.htm. Cited 12. Mar. 2003 (2002)
4. Bondevik, S., Svendsen, J.I., Johnsen, G., Mangerud, J., Kaland, P.E.: The Storrega tsunami along the Norwegian coast, its age and runup. Boreas **26**, 29–53 (1997)
5. McIver, R.D.: Role of naturally occurring gas hydrates in sediment transport. AAPG Bull. **66**, 789–792 (1982)
6. Winters, W.J., Booth, J.S., Mason, D.H., Commeau, R.F., Dillon, W. P.: Laboratory testing of gas hydrates in marine sediment. American Geophysical Union Spring Meeting, Baltimore, April (1995)
7. Westbrook, G.K., Long, C., Peacock, S., Haacke, R., Reston, T., Zillmer, M., Flueh, E., Foucher, J.-P., Nouzé, H., Contrucci, I., Klingelhoefer, F., Best, A.I., Priest, J.A., Camerlenghi, A., Carcione, J., Rossi, G., Madrussani, G., Gei, D., Mienert, J., Vanneste, M., Buenz, S., Hetland, S., Larsen, R., Habetinova, E., Minshull, T.A., Chand, S., Clayton, C.R.I., Dean, S.: Techniques for the Quantification of Methane Hydrate in European Continental Margins – HYDRATECH – Final Report. (2004)
8. Beauchamp, B.: Natural gas hydrates: myths, facts and issues. C. R. Geosci. **336**, 751–765 (2004)
9. Kennett, J.P., Cannariato, K.G., Hendy, I.L., Behl, R.J.: Methane hydrates in quaternary climate change: the clathrate gun hypothesis. AGU, Washington (2003)
10. Gunn, D.A., Nelder, L.M., Rochelle, C.A., Bateman, K., Jackson, P.D., Lovell, M.A., Hobbs, P.R.N., Long, D., Rees, J.G., Schultheiss, P., Roberts, J., Francis, T.: Towards improved ground models for slope instability evaluations through better characterization of sediment-hosted gas-hydrates. Terra Nova **14**, 443–450 (2002)
11. Feeser, V.: Gashydratbildung in Tiefseesedimenten-Zur Rolle der sedimentmechanischen Prozess-Steuereung. DGMK-Tag.Ber. **9706**, 51–60 (1997)
12. Henry, P., Michel, T., Clennell, M.B.: Formation of natural gas hydrates in marine sediments 2. Thermodynamic calculations of stability conditions in porous sediments. J. Geophys. Res. **104** (B10), 23005–23022 (1999)
13. Clennell, M.B., Hovland, M., Booth, J.S., Henry, P., Winters, W.J.: Formation of natural gas hydrates in marine sediments 1. Conceptual model of gas hydrate growth conditioned by host sediment properties. J. Geophys. Res. **104**(B10), 22985–23003 (1999)
14. Booth, J.S., Winters, W.J., Dillon, W.P., Clennell, M.B., Rowe, M. M.: Major occurrences and reservoir concepts of marine clathrate hydrates: implications and field evidence. In: Henriet, J.P., Mienert, J. (eds.) Gas Hydrates; Relevance to World Margin Stability and Climate Change, pp. 275–291. Geological Society of London, London, UK (1998)
15. Brewer, P.G., Orr, F.M., Friederich, G., Kvenvolden, K.A., Orange, D.L., McFarlane, J., Kirkwood, W.: Deep ocean field tests of methane hydrate formation from a remotely operated vehicle. Geology **25**, 407–410 (1997)
16. Egeberg, P.K., Dickens, G.R.: Themodynamic and pore water halogen constraints on gas hydrate distribution at ODP Site 997 (Blake Ridge). Chem. Geol. **153**, 53–79 (1999)
17. Spangenberg, E., Kulenkampff, J., Naumann, R., Erzinger, J.: Pore space hydrate formation in a glass bead sample from methane dissolved water. Geophys. Res. Lett. **32**(L24301), 1–4 (2005)
18. Spangenberg, E.: Modeling of the influence of gas hydrate content on the electrical properties of porous sediments. J. Geophys. Res. **106**(B4), 6535–6548 (2001)
19. Tohidi, B., Anderson, R., Clennell, M.B., Burgass, R.W., Biderkab, A.B.: Visual observation of gas-hydrate formation and dissociation in synthetic porous media by means of glass micromodels. Geology (Boulder) **29**(9), 867–870 (2001)
20. Sills, G.C., Wheeler, S.J., Thomas, S.D., Gardener, T.N.: Behaviour of offshore soils containing gas bubbles. Géotechnique 41(2), 227–241 (1991)
21. van Genuchten, M.T.: A closed-form equation for predicting the hydraulic conductivity of unsaturated soils. Soil Sci. Soc. Am. J. **44**, 892–898 (1980)
22. Cundall, P.A., Strack, O.D.L.: A discrete numerical model for granular assemblies. Géotechnique **29**, 47–65 (1979)
23. Murariu, V., Svoboda, J., Sergeant, P.: The modeling of the separation process in a ferrohydrostatic separator using discrete element method. In: Shimizu, Y., Hart, R., Cundall, P.A. (eds.) Numerical Modeling in Micromechanics via Particle Methods – 2004, pp. 119–126. Balkema Publishers, Leiden (2004)
24. Kawamoto, H.: Introduction of research and development on electromechanics of electromagnetic particles for imaging technology. In: Shimizu, Y., Hart, R., Cundall, P.A. (eds.) Numerical Modeling in Micromechanics via Particle Methods – 2004, pp. 95–101. Balkema Publishers, Leiden (2004)
25. Yao, M., Anandarajah, A.: Three-dimensional discrete element method of analysis of clays. J. Eng. Mech. **129**(6), 585–596 (2003)
26. Gröger, T., Tüzün, U., Heyes, D.M.: Shearing of wet particle systems – discrete element simulation. In: Konietzky, H. (ed.) Numerical Modeling in Micromechanics via Particle Methods, pp. 65–72. Balkema Publishers, Leiden (2003)
27. I. Itasca Consulting Group: PFC2D Particle Flow Code in 2 Dimensions (Version 3.0 Manual). ICG, Minneapolis (2002)
28. Kreiter, S., Feeser, V., Grupe, B.: Numerical simulation of gas hydrate behavior in marine sediments using PFC2D. In: Shimizu, Y., Hart, R., Cundall, P.A. (eds.) Numerical Modeling in Micromechanics via Particle Methods – 2004, pp. 191–197. Balkema Publishers, Leiden (2004)
29. du Noüy, L.P.: A new apparatus for measuring surface tension. J. Gen. Physiol. **1**, 521–524 (1919)
30. Israelachvili, J.N.: Intermolecular and Surface Forces. Academic Press, London (1991)
31. Kreiter, S., Feeser, V.: Mechanics of growing gas hydrates in marine sediments – numerical simulation of sediment–hydrate interaction. 14. Tagung für Ingenieurgeologie, Kiel, Germany, 26–29.3 (2003)
32. Allen, M.P., Tildesley, D.J.: Computer Simulation of Liquids. Oxford University Press, (1987)
33. Uchida, T., Ebinuma, T., Ishizaki, T.: Dissociation condition measurements of methane hydrate in confined small pores of porous glass. J. Phys. Chem. B **103**, 3659–3662 (1999)